

Image Quality Assessment: Integrating Model-Centric and Data-Centric Approaches

Peibei Cao, Dingquan Li, and Kede Ma, *Member, IEEE*

Abstract—Learning-based image quality assessment (IQA) has made remarkable progress in the past decade, but nearly all consider the two key components—model and data—in relative isolation. Specifically, model-centric IQA focuses on developing “better” objective quality methods on fixed and extensively reused datasets, with a great danger of overfitting. Data-centric IQA involves conducting psychophysical experiments to construct “better” human-annotated datasets, which unfortunately ignores current IQA models during dataset creation. In this paper, we first design a series of experiments to probe computationally that such isolation of model and data impedes further progress of IQA. We then describe a computational framework that integrates model-centric and data-centric IQA. As a specific example, we design computational modules to quantify the sampling-worthiness of candidate images based on blind IQA (BIQA) model predictions and deep content-aware features. Experimental results show that the proposed sampling-worthiness module successfully spots diverse failures of the examined BIQA models, which are indeed worthy samples to be included in next-generation datasets.

Index Terms—Learning-based IQA, model-centric IQA, data-centric IQA, sampling-worthiness.

I. INTRODUCTION

Image quality assessment (IQA) is indispensable in a broad range of image processing and computer vision applications, *e.g.*, image acquisition, compression, enhancement, and rendering [1]. In recent years, learning-based methods [2]–[4], especially those using convolutional neural networks (CNNs) [5]–[7] have significantly advanced the field of IQA. A learning-based IQA system generally has two key components: the engine “model” and its fuel “data.” The IQA model is learned to predict image quality from a large number of human-annotated data. From this perspective, it is natural to categorize IQA studies into model-centric and data-centric approaches.

The goal of model-centric IQA [8]–[12] is to build computational methods (*i.e.*, objective models) that provide consistent predictions on human perception of image quality. Improved learning-based IQA models have been developed from the aspects of computational structures, objective functions, and optimization techniques. Particularly, the *computational structures* have shifted from shallow [5] to deep methods with cascaded linear and nonlinear stages [13]. Effective quality

Peibei Cao and Kede Ma are with the Department of Computer Science, City University of Hong Kong, Kowloon, Hong Kong (e-mail: peibeicao20c@my.cityu.edu.hk, kede.ma@cityu.edu.hk).

Dingquan Li is with Network Intelligence Research Department, Peng Cheng Laboratory, Shenzhen, 518066, China (e-mail: dingquanli@pku.edu.cn).

Corresponding author: Kede Ma.

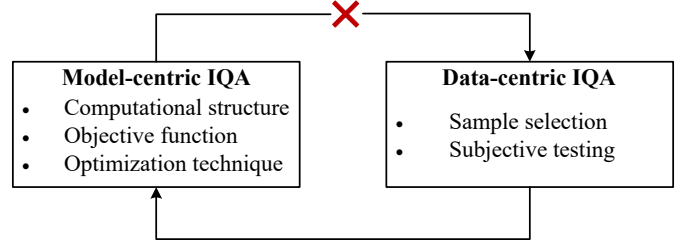


Fig. 1. Past work makes weak connections between data-centric and model-centric IQA, hindering the further progress of the field. The connection from data-centric IQA to model-centric IQA embodies tremendous amount of work on how to train “accurate” IQA models on human-rated datasets. The missing part for closing the loop is to leverage model-centric IQA to guide the design of data-centric IQA, especially in sample selection.

computation operators have also been identified along the way, such as generalized divisive normalization (GDN) over half-wave rectification (ReLU) [6], bilinear pooling over global average pooling [14], and adaptive convolution over standard convolution [11]. The *objective functions* mainly pertain to the formulation of IQA. It is intuitive to think of visual quality as absolute quantity, and employ the Minkowski metric to measure the prediction error. Another popular formulation is learning-to-rank [15] by treating perceptual quality as relative quantity, which admits a family of pairwise and listwise ranking losses [4], [16]. Other loss functions for accelerated convergence [17] and uncertainty quantification [12], [18], have also begun to emerge. The *optimization techniques* in IQA benefit significantly from practical tricks to train large-scale CNNs for visual recognition [19]. One learning strategy specific to IQA is the ranking-based dataset combination trick [12], which enables an IQA model to be trained on multiple datasets without perceptual scale realignment.

The goal of data-centric IQA is to construct human-rated IQA datasets via psychophysical experiments for the purpose of benchmarking and developing objective IQA models. A common theme in data-centric IQA [20]–[23] is to design efficient subjective testing methodologies to collect reliable human ratings of image quality, typically in the form of mean opinion scores (MOSs). Extensive practice [24] seems to show that there is no free lunch in data-centric IQA: collecting more reliable MOSs generally requires more delicate and time-consuming psychophysical procedures, such as the two-alternative forced choice (2AFC) in a well-controlled laboratory environment with proper instructions. Bayesian experimental designs have also been implemented [25], [26] in an attempt to improve rating efficiency. Arguably a more

crucial step in data-centric IQA is sample selection, which is, however, much under-studied. Vonikakis *et al.* [27] proposed a dataset shaping technique to identify the image subset with uniformly distributed attributes of interest. Cao *et al.* [28] described a sample selection method in the context of real-world image enhancement based on the principle of maximum discrepancy competition [29], [30].

Although the past achievements in IQA are worth celebrating, only weak connections have been made between model-centric and data-centric IQA, which we argue is the primary impediment to further progress of IQA (see Fig. 1). From the model perspective, objective methods are optimized and evaluated on fixed (and extensively reused) sets of data, leading to the *overfitting* problem. An excellent example occurs in the subfield of full-reference IQA [1], where objective methods are achieving higher and higher correlation numbers, but fail the naïve test of reference image recovery [31]. From the data perspective, IQA datasets are generally constructed while being blind to existing objective models. This may cause the *easy dataset* problem [23]: the newly created dataset may expose few failures of existing IQA models, resulting in a significant waste of the expensive human labeling budget.

In this paper, we take initial steps towards integrating model-centric and data-centric IQA. Our main contributions are three-folds.

- We design a series of experiments to probe computationally the overfitting problem and the easy dataset problem of blind IQA (BIQA) in real settings.
- We describe a computational framework that integrates model-centric and data-centric IQA. The key idea is to augment the (main) quality predictor with an (auxiliary) computational module to score the sampling-worthiness of candidate images for dataset construction.
- We provide a specific example of this framework, where we start with a (fixed) “top-performing” BIQA model, and train a failure predictor by learning to rank its prediction errors. Our sampling-worthiness module is then the weighted combination of the learned failure predictor and a diversity measure computed as the semantic distance between deep content-aware features [32]. Experiments show that the proposed sampling-worthiness module is able to spot diverse failures of existing BIQA models in comparison to several deep active learning methods [33]–[36]. These samples are indeed worthy of being incorporated into next-generation IQA datasets.

II. RELATED WORK

In this section, we provide a concise overview of model-centric and data-centric IQA. We then briefly describe the unified no-reference image quality and uncertainty evaluator (UNIQUE) [12], as we will rely heavily on it to demonstrate the proposed framework.

A. Model-Centric IQA

We will focus on reviewing model-centric BIQA, which improves quality prediction from the model perspective without reliance on original undistorted images. Conventional BIQA

models pre-defined non-learnable *computational structures* to extract natural scene statistics (NSS). Learning occurred at the quality regression stage by fitting a mapping from NSS to MOSs. Commonly, NSS were extracted in the transform domain [37], [38], where the statistical irregularities can be more easily characterized. Nevertheless, transform-based methods were usually very slow, which motivated BIQA models in the spatial domain, *e.g.*, BRISQUE [8] and CORNIA [2].

With the latest advances in CNNs, learnable computational structures based on stages of linear convolution, downsampling, and nonlinear activation have revolutionized the field of BIQA [9]–[12]. Along this line, the *objective functions* play an important role in guiding the optimization of BIQA models. It is straightforward to formulate BIQA as regression, and the Minkowski metric is the objective function of choice. An alternative view of BIQA is through the lens of learning-to-rank [16], with the goal of inferring relative rather than absolute quality. Pairwise learning-to-rank objectives such as the cross entropy [4] and the fidelity [39] losses, and listwise objectives such as the cross entropy over permutation probabilities [4] and the Pearson linear correlation [17] have been successfully adopted. One last ingredient of model-centric IQA is the selection of *optimization techniques* for effective model training, especially when the human-rated IQA data are scarce. Fine-tuning from pre-trained CNNs on other vision tasks [10], patchwise training [7], and quality-aware pre-training [11] are practical optimization tricks in BIQA. Of particular interest is the unified optimization strategy by Zhang *et al.* [12], allowing a single model to learn from multiple datasets simultaneously.

The success of model-centric BIQA was established on the same datasets [20], [22], [40], [41], which have been used to compare BIQA models for quite many years. Thus, it is reasonable to conjecture that the impressive correlation numbers achieved by sophisticated computational structures and optimization techniques may be a consequence of overfitting, and need more cautious analysis.

B. Data-Centric IQA

Data-centric IQA improves the quality prediction performance from the data perspective, and consists of two major steps: sample selection and subjective testing. The immediate output is a human-rated dataset for training and benchmarking objective IQA models. For a long time, the research focus of data-centric IQA has been designing reliable and efficient *subjective testing* methodologies for MOS collection [42], [43]. It is generally believed that the 2AFC design (also known as paired comparison) in a well-controlled laboratory environment is more reliable than single-stimulus and multiple-stimulus methods. However, the cost to exhaust all paired comparisons scales quadratically with the number of images in the dataset, and is prohibitively expensive when the image size is large. Several methods have been introduced to reduce the cost of the 2AFC design, including HodgeRank [25] and Bayesian experimental designs [26]. To further accelerate the process, crowdsourcing-based single-stimulus methods [22], [44] have been practiced to build large-scale IQA datasets with relatively noisier MOSs.

Sample selection is perhaps more crucial in data-centric IQA, but experiences much less success. Early datasets, such as LIVE [20], TID2008 [45], and CSIQ [40], selected images with simulated distortions. Due to the combination of reference content, distortion type and level, the number of distinct reference images is often limited. Recent large-scale IQA datasets began to contain images with realistic camera distortions, including CLIVE [22], KonIQ-10k [13], SPAQ [23], and PaQ-2-PiQ [46]. Such shift in sample selection provides a good test for synthetic-to-realistic generalization.

Sample diversity during dataset creation has also been taken into account. Vonikakiset *et al.* [27] cast sample diversity as a mixed integer linear programming, and selected a dataset with uniformly distributed image attributes (*e.g.*, brightness, colorfulness, contrast, and sharpness). Euclidean distances between deep features [13], [28] are also used to measure the semantic similarity. Nevertheless, sample diversity is only one piece of the story; often, the included images are too easy to challenge existing IQA models. For example, Fang *et al.* [23] took nearly one year to create the SPAQ dataset consisting of more than 11,000 images, most of which turn out to be easy examples, and pose little challenge to current BIQA models (see Sec. III-B).

Active learning [47], [48] may come naturally into play to prioritize sample selection. Wang *et al.* [49] spotted the failures of a BIQA model with the help of multiple full-reference IQA methods in the setting of synthetic distortions. They [50] later extended the idea to the authentic distortion scenario by creating a set of self-competitors via network pruning. The two methods are algorithm-specific, and may not be generalized to existing BIQA models. Other active learning strategies such as uncertainty-based sampling [51], query by committee [52], expected model change maximization [53], and failure prediction [54], [55] may be applied. Nevertheless, it remains to be seen whether these strategies are feasible and, if so, how effective they are in the context of deep learning-based IQA.

C. UNIQUE

UNIQUE [12] is a recently proposed BIQA model, which combines multiple IQA datasets as the training data. Specifically, assuming Gaussianity of the true perceptual quality $q(x)$ with mean $\mu(x)$ and variance $\sigma^2(x)$ and the independence of quality variability across images, the probability of image x having higher perceptual quality than image y can be calculated as

$$p(x, y) = \Pr(q(x) \geq q(y)) = \Phi\left(\frac{\mu(x) - \mu(y)}{\sqrt{\sigma^2(x) + \sigma^2(y)}}\right), \quad (1)$$

where $\Phi(\cdot)$ denotes the standard Gaussian cumulative distribution function. From the i -th dataset for a total of N datasets, UNIQUE randomly samples N_i pairs of images $\{(x_j^{(i)}, y_j^{(i)})\}_{j=1}^{N_i}$, and the combined training dataset is thus in the form of $\mathcal{D} = \{\{(x_j^{(i)}, y_j^{(i)}), p_j^{(i)}\}_{j=1}^{N_i}\}_{i=1}^N$.

UNIQUE aims to learn two differentiable functions $f_w(\cdot)$ and $\sigma_w(\cdot)$, parameterized by a vector w , for quality and uncertainty estimation. The prediction of $p(x, y)$ in Eq. (1)

TABLE I
SRCC BETWEEN THE PERFORMANCE RANKING OF NINE BIQA METHODS AND THEIR PUBLISHING TIME ON FOUR DATASETS. IT IS CLEAR THAT THE QUALITY PREDICTION PERFORMANCE “IMPROVES” STEADILY OVER TIME

Dataset	BID [21]	CLIVE [22]	KonIQ-10k [22]	SPAQ [23]
SRCC	0.6946	0.7950	0.6695	0.7029

can be done by replacing $\mu(\cdot)$ and $\sigma(\cdot)$ with their respective estimates:

$$\hat{p}(x, y) = \Phi\left(\frac{f_w(x) - f_w(y)}{\sqrt{\sigma_w^2(x) + \sigma_w^2(y)}}\right). \quad (2)$$

UNIQUE minimizes the fidelity loss [39] between the two probability distributions $p(x, y)$ and $\hat{p}(x, y)$ for parameter optimization:

$$\ell(x, y, p) = 1 - \sqrt{p(x, y)\hat{p}(x, y)} - \sqrt{(1 - p(x, y))(1 - \hat{p}(x, y))}. \quad (3)$$

To resolve the scaling ambiguity in Eq. (2) and to resemble the human uncertainty when perceiving digital images, UNIQUE adds a hinge-like regularizer during training [12]. The original UNIQUE employs ResNet-34 [56] as the backbone followed by bilinear pooling and ℓ_2 -normalization, and implements $f_w(\cdot)$ and $\sigma_w(\cdot)$ as the two outputs of a fully connected (FC) layer.

III. PROBING PROBLEMS IN THE PROGRESS OF BIQA

In this section, we design a series of experiments to probe computationally that the *overfitting* problem and the *easy dataset* problem have actually emerged in the current development of BIQA, which we attribute to the weak connections between model-centric and data-centric BIQA.

A. Overfitting Problem

As there is no standardized computable definition of overfitting, especially in the context of deep learning [58], quantifying overfitting is still a wide open problem. Here we choose to use the group maximum differentiation (gMAD) competition [59] to probe the generalization of BIQA models to a large-scale unlabeled dataset. gMAD is a discrete instantiation of the MAD competition [29] that relies on synthesized images to optimally distinguish the models. As opposed to the *average-case* performance measured on existing IQA datasets, say by Spearman’s rank correlation coefficient (SRCC), gMAD can be seen as a *worst-case* performance test by comparing the models using extremal image pairs that are likely to falsify them. We declare an overfitting case of a BIQA model if it shows strong average performance on standard IQA datasets but weak performance in the gMAD competition.

a) *Experimental Setup*: We choose nine BIQA models from 2017 to 2021: RankIQA [9], DeepIQA [7], NIMA [10], KonCept512 [13], Fang2020 [23], HyperIQA [11], LinearityIQA [17], UNIQUE [12], and MetaIQA+ [57]. Table I shows the SRCC results between the publishing time of the

TABLE II

RANKING RESULTS OF NINE BIQA MODELS. A SMALLER RANK INDICATES BETTER PERFORMANCE. “DISTRIBUTION” IN THE THIRD COLUMN MEANS THAT NIMA USES THE EARTH MOVER’S DISTANCE TO MATCH THE GROUND-TRUTH AND PREDICTED 1D QUALITY DISTRIBUTIONS. “ALL” IN THE FOURTH COLUMN INDICATES THAT UNIQUE IS TRAINED ON THE COMBINED DATASET OF LIVE, CSIQ, KADID-10K, BID, CLIVE, AND KONIQ-10K

Name	Backbone	Formulation	Training Set	Publishing Time	SRCC Rank	gMAD Rank	Δ Rank
UNIQUE [12]	ResNet-34	Ranking	All	2021.03	1	5	-4
KonCcept512 [13]	InceptionResNetV2	Regression	KonIQ-10k	2020.01	2	1	1
HyperIQA [11]	ResNet-50	Regression	KonIQ-10k	2020.08	3	2	1
LinearityIQA [17]	ResNeXt-101	Regression	KonIQ-10k	2020.10	4	3	1
MetalIQA+ [57]	ResNet-18	Regression	CLIVE	2021.04	5	8	-3
Fang2020 [23]	ResNet-50	Regression	SPAQ	2020.08	6	9	-3
NIMA [10]	VGG-16	Distribution	AVA	2018.04	7	4	3
DeepIQA [7]	VGG-like CNN	Regression	LIVE	2018.01	8	7	1
RankIQA [9]	VGG-16	Ranking	LIVE	2017.12	9	6	3

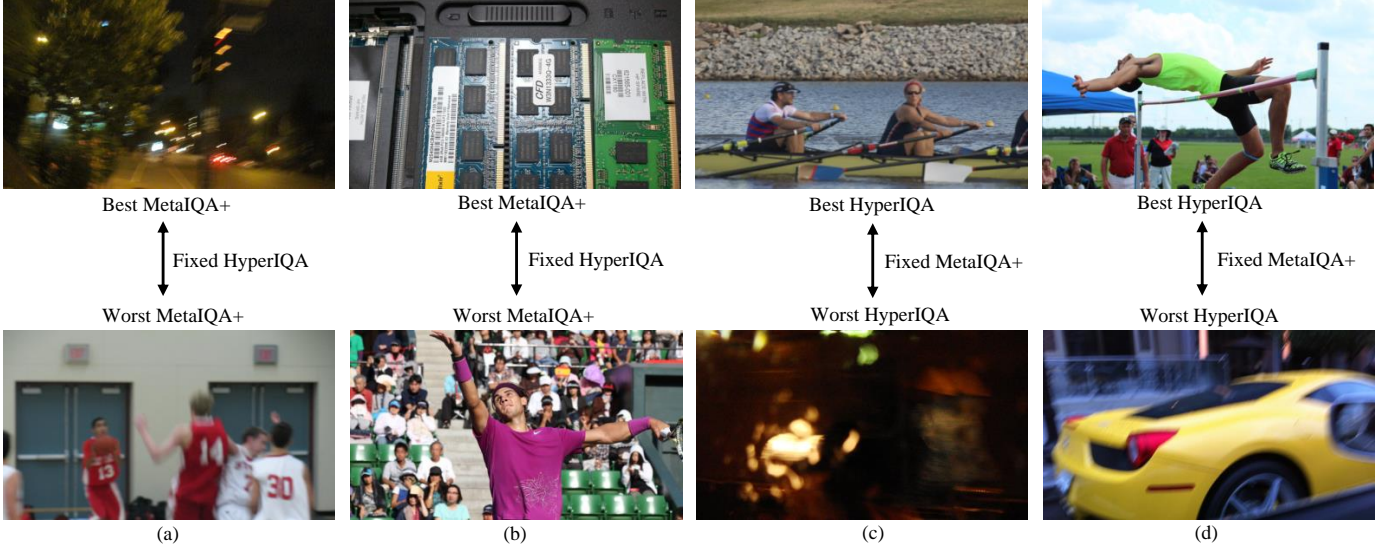


Fig. 2. Representative gMAD pairs between HyperIQA and MetalIQA+. (a) Fixing HyperIQA at the low quality level. (b) Fixing HyperIQA at the high quality level. (c) Fixing MetalIQA+ at the low quality level. (d) Fixing MetalIQA+ at the high quality level.

algorithms and their performance ranking¹ on four widely used IQA datasets, BID [21], CLIVE [22], KonIQ-10k [13], and SPAQ [23]. We find that “steady progress” over the years has been made by employing more complicated computational structures and more advanced optimization techniques.

We now set the stage for the nine BIQA models to perform gMAD competition. Specifically, we first gather a large-scale unlabeled dataset \mathcal{U} , containing 100,000 photographic images with marginal distributions nearly uniform w.r.t. five image attributes (*i.e.*, JPEG compression ratio, brightness, colorfulness, contrast, and sharpness). Our dataset covers a wide range of realistic camera distortions, such as sensor noise contamination, motion and out-of-focus blur, under- and over-exposure, contrast reduction, color cast, and a mixture of them. Given two BIQA models $f_i(\cdot)$ and $f_j(\cdot)$, gMAD [59] selects top- K image pairs that best discriminate between them:

$$(x_k^*, y_k^*) = \arg \max_{x, y} f_i(x) - f_i(y) \\ \text{s.t. } f_j(x) = f_j(y) = \alpha, x, y \in \mathcal{U} \setminus \mathcal{D}_{k-1}, \quad (4)$$

¹As each BIQA model assumes different (and unknown) training and testing splits, for a less biased comparison, we compute the quality prediction performance on the full dataset.

where $\mathcal{D}_{k-1} = \{x_{k'}^*, y_{k'}^*\}_{k'=1}^{k-1}$ is the current gMAD image set. The k -th image pair must lie on the α -level set of f_j , where α specifies a quality level. The roles of f_i and f_j should be switched. Q (non-overlapping) quality levels are selected to cover the full quality spectrum. By exhausting all distinct pairs of BIQA models and quality levels, we arrive at a gMAD set \mathcal{D} that contains a total of $9 \times 8 \times 5 \times 2 = 720$ image pairs, where we set $Q = 5$ and $K = 2$.

We invite 25 human subjects to gather perceived quality judgments of each gMAD pair using the 2AFC method. They are forced to choose the image with higher perceived quality for the 720 paired comparisons. The 25 subjects are mostly young researchers (age between 22 and 30) with a computer science background, but are unaware of the goal of this work, including 12 male and 13 female subjects. They are asked to finish the experiments in an office environment with a normal lighting condition and without reflecting ceiling walls and floors. The LCD monitor has a resolution of 2560×1600 pixels, which is sufficient to display the image pairs simultaneously in the random spatial and temporal order. The subjects can move closer to and farther away from the display for better distortion visibility. No time constraint is enforced, and the participants can take a break at any time to minimize the



Fig. 3. Representative gMAD pairs between HyperIQA and LinearityIQA. (a) Fixing HyperIQA at the low quality level. (b) Fixing HyperIQA at the high quality level. (c) Fixing LinearityIQA at the low quality level. (d) Fixing LinearityIQA at the high quality level.

TABLE III
DETAILED TRAINING SPECIFICATIONS OF UNIQUE VARIANTS FOR PROBING THE EASY DATASET PROBLEM

Variant	[Training] / [Test] Datasets	[#Training Pairs] / [#Test Images]
UNIQUEv1	[BID] / [CLIVE, KonIQ-10k, SPAQ]	[20,000] / [1,162, 10,073, 11,125]
UNIQUEv2	[BID, CLIVE] / [KonIQ-10k, SPAQ]	[20,000, 40,000] / [10,073, 11,125]
UNIQUEv3	[BID, CLIVE, KonIQ-10k] / [SPAQ]	[20,000, 40,000, 90,000] / [11,125]

influence of the fatigue effect [42].

After subjective testing, we obtain the raw pairwise comparison matrix $A \in \mathbb{R}^{9 \times 9}$, where $a_{ij} \in \{0, 1, \dots, 250\}$ indicates the counts of x^* preferred over y^* by the 25 subjects on the ten associated image pairs (by solving Problem (4)). We compute, from A , a second matrix $B \in \mathbb{R}^{9 \times 9}$, where $b_{ij} = a_{ij}/a_{ji}$ denotes the pairwise dominance of f_i over f_j . Laplace smoothing [60] is applied when a_{ji} is close to zero. We convert the pairwise comparisons into a global ranking $r \in \mathbb{R}^9$ using Perron rank [61]:

$$r = \lim_{t \rightarrow \infty} \frac{1}{t} \sum_{\beta=1}^t \frac{B^\beta}{\mathbf{1}^T B^\beta \mathbf{1}}, \quad (5)$$

where $\mathbf{1}$ is a 9-dimensional vector of all ones. The solution to Eq. (5) is the normalized eigenvector of B corresponding to the largest eigenvalue. A larger r_i indicates better performance of f_i in the gMAD competition.

b) Results: Table II compares the ranking results of the nine BIQA models in the gMAD competition and in terms of the average SRCC on the four full datasets, BID [21], CLIVE [22], KonIQ-10k [13], and SPAQ [23]. The primary observation is that the latest published models, such as UNIQUE [12], MetaIQA+ [57], and Fang2020 [23] tend to overfit the peculiarities of the training sets with advanced optimization techniques. In particular, UNIQUE learns to rank image pairs from all available datasets, MetaIQA+ adopts deep meta learning for unseen distortion generalization, while Fang2020 enables adaptive multi-task learning for incorpora-

tion of auxiliary quality-relevant information. They rank much higher in terms of average SRCC than in gMAD.

Compared to improving upon optimization techniques, selecting computational structures with more capacity² as the backbones seems to be a wiser choice, as evidenced by KonCept512, HyperIQA, and LinearityIQA with high rankings in gMAD. Fig. 2 shows such a visual comparison of the representative gMAD pairs between MetaIQA+ based on ResNet-18 and HyperIQA based on ResNet-50. Pairs of images in (a) and (b) have similar quality according to human perception, which is consistent with HyperIQA. When the roles of HyperIQA and MetaIQA+ are reversed, it is clear that the pairs of images in (c) and (d) exhibit substantially different quality. HyperIQA correctly predicts top images to have much better quality than bottom images, and meanwhile, the weaknesses of MetaIQA+ in handling dark and blurry scenes have also been exposed. Nevertheless, purely increasing the capacity of the backbone does not necessarily lead to consistent improvements in quality prediction, which again may be a consequence of potential overfitting. For example, HyperIQA identifies content-adaptive convolution to be a more quality-relevant computation. With ResNet-50 as the backbone, it is able to outperform LinearityIQA with a more powerful ResNeXt-101 (see Fig. 3).

In addition, compared to SPAQ, KonIQ-10k of a similar scale serves as a more suitable training set, on which

²As all backbone architectures are originally proposed for ImageNet classification, we thus conveniently regard the ImageNet validation accuracy as a rough indication of model capacity.

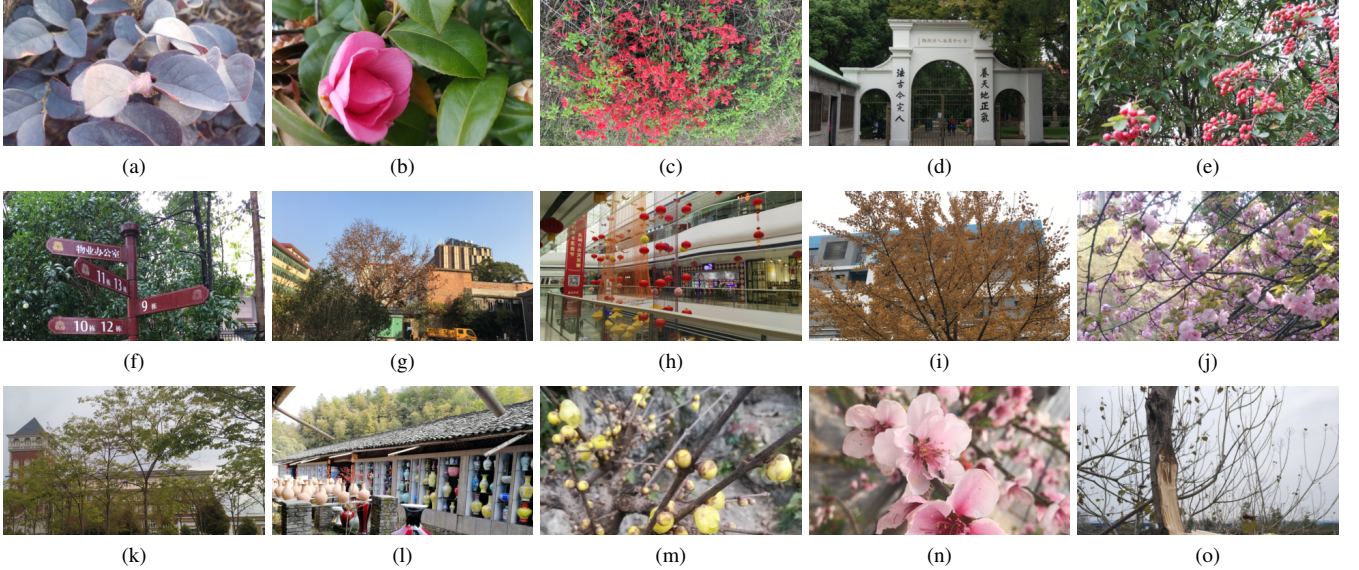


Fig. 4. The top-5 difficult samples in SPAQ, as measured by the MSEs between model predictions and MOSs: (a)-(e) for UNIQUEv1. (f)-(j) for UNIQUEv2. (k)-(o) for UNIQUEv3. We expect such samples to be visually diverse in terms of the content and distortion types in order to expose different failure scenarios of UNIQUEs, which is unfortunately not observed.

more generalizable models can be learned. More surprisingly, Fang2020 [23] trained on SPAQ even underperforms NIMA and DeepIQA, which are, respectively, trained on datasets of aesthetic and synthetic image quality. This provides a strong indication that how overfitting can emerge if a training set is not well prepared. This issue is also closely related to the easy dataset problem, which will be deeply investigated in the next subsection. In summary, the SRCC between the gMAD ranking of the BIQA models and their publishing time is only 0.0753, implying that the progress made by model-centric IQA might be somewhat over-estimated in terms of real-world generalization.

B. Easy Dataset Problem

In order to reveal the easy dataset problem, it suffices to empirically show that the newly created datasets are less effective in falsifying current BIQA models.

a) Experimental Setup: We work with the same four datasets - BID [21], CLIVE [22], KonIQ-10k [13], and SPAQ [23]. To achieve our goal, we select a state-of-the-art BIQA model - UNIQUE [12] - that permits training on multiple datasets. We train three UNIQUEs (*i.e.*, UNIQUEv1, UNIQUEv2, and UNIQUEv3, respectively) on the combination of available datasets in chronological order. For each training setting, we randomly sample 80% images from each dataset to construct the training set, leaving the remaining 10% for validation and 10% for testing. To reduce the bias caused by the randomness in dataset splitting, we repeat the training procedure ten times, and report the median SRCC results for UNIQUE variants. Detailed training specifications can be found in Table III.

b) Results: Table IV lists the SRCC results between predictions of UNIQUEs and MOSs of different IQA datasets as test sets. The primary observation is that as more datasets

TABLE IV
SRCC BETWEEN PREDICTIONS OF UNIQUES AND MOSs OF DIFFERENT TEST SETS. “—” MEANS THAT THE CORRESPONDING DATASET IS USED FOR JOINTLY TRAINING

SRCC	UNIQUEv1	UNIQUEv2	UNIQUEv3
CLIVE [22]	0.6998	—	—
KonIQ-10k [13]	0.6917	0.7251	—
SPAQ [23]	0.7204	0.7932	0.8112

are available for training, the newly created ones are more difficult to challenge the most recent UNIQUE. For example, trained on the combination of BID, CLIVE, and KonIQ-10k, UNIQUEv3 achieves a satisfactory SRCC of 0.8112 on SPAQ, which is higher than 0.7932 and 0.7204 for UNIQUEv2 and UNIQUEv1 trained with fewer data. Although SPAQ is the latest dataset, it is easier than CLIVE and KonIQ-10k. This is supported by the highest correlations obtained by UNIQUEv1 and UNIQUEv2 on SPAQ. These results are consistent with the observations in Sec. III-A, where models trained on KonIQ-10k and CLIVE rank higher than models trained on SPAQ. What is worse, the most difficult examples (as measured by the mean squared error (MSE) between model predictions and MOSs) often share similar visual appearances (see visual examples in Fig. 4). This shows that the sample diversity and difficulty of existing datasets may not be well imposed in a principled way.

IV. PROPOSED FRAMEWORK FOR INTEGRATING MODEL-CENTRIC AND DATA-CENTRIC IQA

In this section, we describe a computational framework for integrating model-centric and data-centric IQA approaches, and provide a specific instance within the framework to alleviate the overfitting and easy dataset problems.

Algorithm 1: Computational Framework for Integrating Model-Centric and Data-Centric IQA

Input: A training set \mathcal{L} , a large-scale unlabeled image set \mathcal{U} , an off-the-shelf BIQA model $f^{(0)}(\cdot)$ (with the associated loss function and optimization technique), a difficulty measure $\text{Diff}(\cdot)$, a diversity measure $\text{Div}(\cdot)$, and the maximum iteration number T

Output: T new datasets $\{\mathcal{D}^{(t)}\}_{t=1}^T$, and a rectified IQA model $f^{(T)}$

```

1 for  $t \leftarrow 1$  to  $T$  do
2    $\mathcal{U} \leftarrow \mathcal{U} \setminus \left( \bigcup_{t'=1}^{t-1} \mathcal{D}^{(t')} \right)$ 
3    $\mathcal{D}^{(t)} = \arg \max_{\mathcal{S} \subset \mathcal{U}} \text{Diff}(\mathcal{S}; f^{(t-1)}) + \lambda \text{Div}(\mathcal{S})$ 
4   Collect the MOS for each  $x \in \mathcal{D}^{(t)}$  in an assumed subjective testing environment
5   Train  $f^{(t)}$  (or fine-tune  $f^{(t-1)}$  to obtain  $f^{(t)}$ ) on the combination of  $\mathcal{L}$  and  $\bigcup_{t'=1}^t \mathcal{D}^{(t')}$ 
6 end

```

A. Proposed Framework

As shown in Fig. 1, there is a rich body of work on how to train IQA models on available human-rated datasets, *i.e.*, the connection from data-centric IQA to model-centric IQA. The missing part for closing the loop is to leverage existing IQA models to guide the creation of new IQA datasets. Assuming that a subjective testing environment exists, in which reliable MOSs can be collected, the problem reduces to how to sample, from a large-scale unlabeled dataset \mathcal{U} with great scene complexities and visual distortions, a subset \mathcal{D} , whose size is constrained by the human labeling budget. Motivated by the experimental results in Sec. III, we argue that the images in \mathcal{D} are *sampling-worthy* if they are

- *difficult*, which best manifest themselves as dramatic failures of state-of-the-art IQA models,
- and *diverse*, which test different aspects of the models, therefore exposing different erroneous behaviors.

Mathematically, sample selection corresponds to the following optimization problem:

$$\mathcal{D} = \arg \max_{\mathcal{S} \subset \mathcal{U}} \text{Diff}(\mathcal{S}; f) + \lambda \text{Div}(\mathcal{S}), \quad (6)$$

where $\text{Diff}(\cdot)$ is a difficulty measure of \mathcal{S} w.r.t. the IQA model, $f(\cdot)$. It is straightforward to define $\text{Diff}(\cdot)$ on a set of IQA algorithms as well. $\text{Div}(\cdot)$ quantifies the diversity of \mathcal{S} . λ is a trade-off parameter for the two terms. As a specific case of subset selection [62], [63], Problem (6) is generally NP-hard unless special properties of $\text{Diff}(\cdot)$ and $\text{Div}(\cdot)$ can be exploited. Popular approximate solutions to subset selection include greedy algorithms and convex relaxation methods.

Once \mathcal{D} is identified, we collect the MOS for each $x \in \mathcal{D}$ in the assumed subjective testing environment, which makes the connection from model-centric IQA to data-centric IQA. The newly labeled \mathcal{D} , by construction, exposes different failures of the IQA model $f(\cdot)$, which is in turn useful for improving its generalization. We then iterate the process of model rectification, sample selection, and subjective testing, with the ultimate

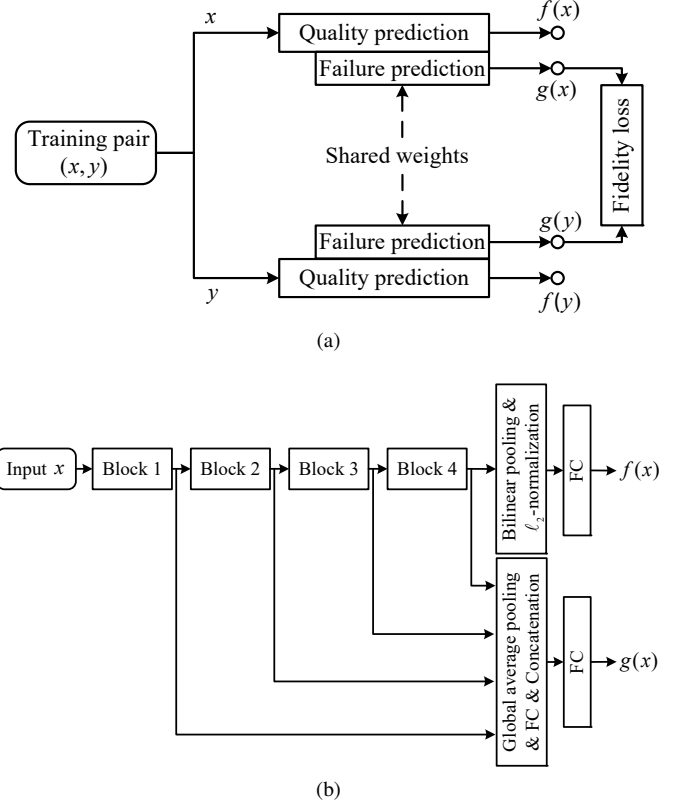


Fig. 5. (a) The main quality predictor, $f(\cdot)$, is fixed and the auxiliary failure predictor, $g(\cdot)$, is optimized by minimizing the fidelity loss. (b) The backbone of $f(\cdot)$ is ResNet-34, composed of four residual blocks. The failure predictor $g(\cdot)$ accepts the pooled feature representations from the four blocks, and produces a scalar to indicate the learning difficulty of the input image.

goal of improving learning-based IQA from both model and data perspectives. We summarize the proposed computational framework in Algorithm 1.

B. A Specific Instance in BIQA

In this subsection, we provide a specific instance of the proposed computational framework, and demonstrate its feasibility in integrating model-centric and data-centric BIQA.

To better contrast with the results in Sec. III-B and to reduce the load of subjective testing, we use SPAQ to simulate the large-scale unlabeled dataset \mathcal{U} . The off-the-shelf BIQA model for demonstration is again UNIQUE [12], which trains on the combination of the full BID, CLIVE, and KonIQ-10k as \mathcal{L} .

The core of our method is the instantiation of the sampling-worthiness module, which consists of two computational sub-modules to quantify the difficulty of a candidate set \mathcal{S} w.r.t. to $f(\cdot)$ and the diversity of \mathcal{S} . Inspired by previous seminal work [64]–[67], we choose to measure the difficulty through failure prediction. As shown in Fig. 5, our failure predictor, $g(\cdot)$, has two characteristics: 1) it is an auxiliary module that incurs a small number of parameters; 2) it can either be solely trained while holding the quality predictor $f(\cdot)$ fixed or jointly trained along with $f(\cdot)$. Recall that our goal is to expose diverse failures of existing BIQA models, and thus it is preferred not to re-train or fine-tune $f(\cdot)$. For the main

TABLE V
CONVOLUTIONAL ARCHITECTURE OF RESNET-34 [56] AS THE BACKBONE OF THE QUALITY AND FAILURE PREDICTORS. THE NONLINEARITY AND NORMALIZATION ARE OMITTED FOR BREVITY

Layer Name	Network Parameter
Convolution	$7 \times 7, 64$, stride 2
Max Pooling	3×3 , stride 2
Block 1	$\left[\begin{array}{c} 3 \times 3, 64, \text{stride 1} \\ 3 \times 3, 64, \text{stride 1} \end{array} \right] \times 3$
Block 2	$\left[\begin{array}{c} 3 \times 3, 128, \text{stride 2} \\ 3 \times 3, 128, \text{stride 1} \end{array} \right] \times 1$
	$\left[\begin{array}{c} 3 \times 3, 128, \text{stride 1} \\ 3 \times 3, 128, \text{stride 1} \end{array} \right] \times 3$
Block 3	$\left[\begin{array}{c} 3 \times 3, 256, \text{stride 2} \\ 3 \times 3, 256, \text{stride 1} \end{array} \right] \times 1$
	$\left[\begin{array}{c} 3 \times 3, 256, \text{stride 1} \\ 3 \times 3, 256, \text{stride 1} \end{array} \right] \times 5$
Block 4	$\left[\begin{array}{c} 3 \times 3, 512, \text{stride 2} \\ 3 \times 3, 512, \text{stride 1} \end{array} \right] \times 1$
	$\left[\begin{array}{c} 3 \times 3, 512, \text{stride 1} \\ 3 \times 3, 512, \text{stride 1} \end{array} \right] \times 2$

experiments, we choose to fix the quality predictor, and defer the case of joint training in Sec. IV-D.

The failure predictor $g(\cdot)$ accepts the feature maps of the input image x from each *fixed* residual block (see details in Table V) as inputs, and summarizes spatial information via global average pooling. Each stage of pooled features then undergo an FC layer with the same number of output channels, C , followed by ReLU nonlinearity. After that, the four feature vectors of the same length are concatenated to pass through another FC layer to compute a scalar $g(x)$ as the indication of the difficulty of learning x . Assuming Gaussianity of $g(x)$ with unit variance, the probability that x is more difficult than y is calculated by

$$\hat{p}_F(x, y) = \Phi\left(\frac{g(x) - g(y)}{\sqrt{2}}\right). \quad (7)$$

For the same training pair (x, y) , the ground-truth label can be computed by

$$p_F(x, y) = \begin{cases} 1 & \text{if } |f(x) - \mu(x)| \geq |f(y) - \mu(y)| \\ 0 & \text{otherwise,} \end{cases} \quad (8)$$

where $\mu(\cdot)$ represents the MOS. That is, $p_F(x, y) = 1$ indicates that x is more difficult to learn than y , as evidenced by a higher absolute error. We learn the parameters of the failure predictor (*i.e.*, five FC layers) by minimizing the fidelity loss between $p_F(x, y)$ and $\hat{p}_F(x, y)$:

$$\ell(x, y, p_F) = 1 - \sqrt{p_F(x, y)\hat{p}_F(x, y)} - \sqrt{(1 - p_F(x, y))(1 - \hat{p}_F(x, y))}. \quad (9)$$

One significant advantage of the learning-to-rank formulation of failure prediction is that $g(\cdot)$ is independent of the scale of $f(\cdot)$, which may oscillate over iterations [67] if joint training

is enabled. After sufficient training, we may adopt $g(\cdot)$ to quantify the difficulty of \mathcal{S} :

$$\text{Diff}(\mathcal{S}) = \frac{1}{|\mathcal{S}|} \sum_{x \in \mathcal{S}} g(x), \quad (10)$$

where $|\mathcal{S}|$ denotes the cardinality of the set \mathcal{S} .

We next define the diversity of \mathcal{S} as the mean pairwise distances computed from the 1,000-dim logits of the VGGNet [32]:

$$\text{Div}(\mathcal{S}) = \frac{1}{|\mathcal{S}|^2} \sum_{(x, y) \in \mathcal{S}} \|\text{logit}(x) - \text{logit}(y)\|_2^2, \quad (11)$$

which provides a reasonable account for the semantic dissimilarity. While maximizing $\text{Diff}(\mathcal{S})$ in Eq. (10) enjoys a linear complexity in the problem size, it is not the case when maximizing $\text{Div}(\mathcal{S})$ [68]. To facilitate subset selection, we use a similar greedy method (in Eq. (4)) to solve Problem (6). Assuming $\mathcal{D} = \{x_{k'}^*\}_{k'=1}^{k-1}$ is the (sub)-optimal subset that contains $k-1$ images, the k -th optimal image can be chosen by

$$x_k^* = \arg \max_{x \in \mathcal{U} \setminus \mathcal{D}} g(x) + \frac{\lambda}{k-1} \sum_{k'=1}^{k-1} \|\text{logit}(x) - \text{logit}(x_{k'}^*)\|_2^2. \quad (12)$$

C. Experiments

a) *Experimental Setup*: Training is carried out by minimizing the fidelity loss in Eq. (9) for failure prediction while fixing the quality predictor. The output channel of the four FC layers for feature projection is set to $C = 128$. All five FC layers in $g(\cdot)$ are initialized by He's method [69]. We adopt Adam [70] with a mini-batch size of 32, an initial learning rate of 10^{-4} and a decay factor of 10 for every five epochs, and we train the failure predictor for fifteen epochs. During sample selection, we set the λ in Eq. (6) to 10^{-6} in order to balance the scale difference between $\text{Diff}(\cdot)$ and $\text{Div}(\cdot)$. We use SPAQ to simulate \mathcal{U} , and select a subset \mathcal{D} of size 100. Similarly, we repeat the training procedure five times to reduce the influence of random initializations, and report the median results. We compare the failure identification capability of the proposed sampling-worthiness module against several deep active learning methods, including random sampling, sampling by representativeness-diversity [36], UNIQUE uncertainty [12], query by committee [52], coreset selection [34], and MC dropout [33]. The setups of the competing methods are summarized as follows.

- For random sampling as the baseline, 100 images are uniformly sampled from the unlabeled dataset \mathcal{U} .
- For sampling by representativeness-diversity, k -means clustering is performed in the bilinearly pooled and ℓ_2 -normalized feature space. For the i -th iteration where $i = \{1, \dots, 100\}$, we perform k -means clustering on \mathcal{U} , where $k = i$. We identify the largest cluster that does not contain previously selected images as the current most representative cluster³, from which the image with the minimum distance to its centroid is sampled.

³Note that such cluster always exists because the number of clusters is larger than the number of already selected images in each iteration.

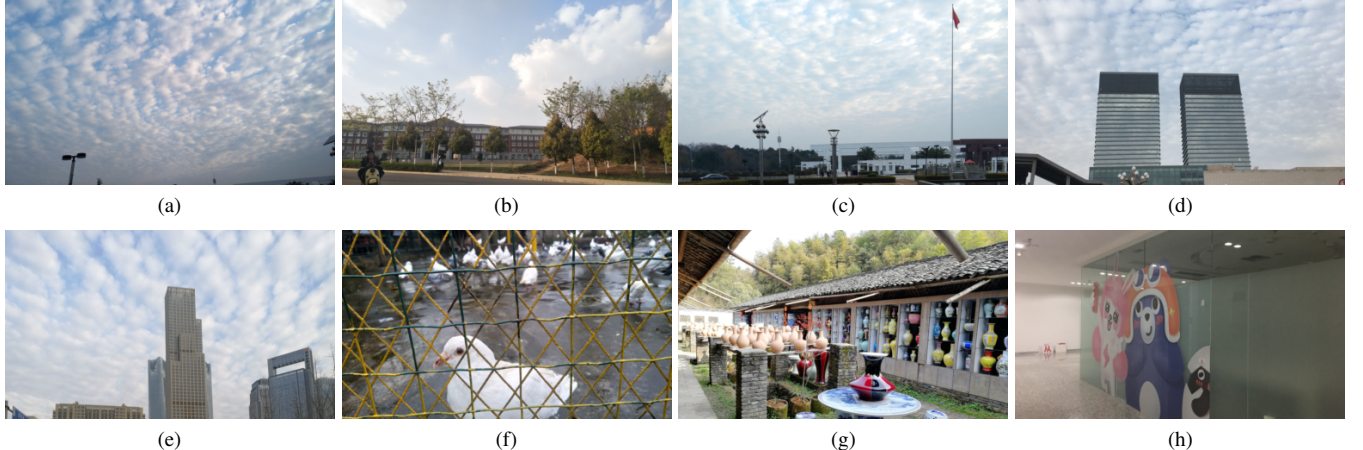


Fig. 6. Representative images selected from SPAQ by the proposed sampling-worthiness module. (a)-(d)/(e)-(h) are selected images without/with the diversity measure. Zoom in for improved distortion visibility.

- The UNIQUE model comes with a trained uncertainty estimator $\sigma_w(\cdot)$ (see Eq. (2)). We directly maximize it for sample selection.
- For query by committee, we obtain fifteen augmented versions of the input image by randomly flipping, resizing, and cropping. The prediction variance acts as the $\text{Diff}(\cdot)$ in Eq. (6).
- For core-set selection, we employ the bilinearly pooled and ℓ_2 -normalized feature vector as the image representation, and iteratively select images with the maximum distances to the sampled dataset \mathcal{D} in the representation space. Here, the image-to-set distance is defined as the minimum Euclidean distance between the image and all images in \mathcal{D} . It is important to note that the diversity measure defined in Eq. (11) differs from core-set selection in 1) feature representation (VGG-based content representation against UNIQUE-based quality representation) and 2) image-to-set distance calculation.
- For MC dropout, we randomly dropout the bilinearly pooled and ℓ_2 -normalized feature vector for fifteen times at a dropout rate $p = 0.5$. The prediction variance is used to replace $\text{Diff}(\cdot)$ in Eq. (6). Although the original UNIQUE does not include dropout during training, we empirically verify that the incorporation of dropout as post-processing does not hurt its quality prediction performance, where an SRCC of 0.8383 between mean predictions and MOSs has been observed.

b) Failure Identification Results: Table VI shows the SRCC results between UNIQUE predictions and MOSs on the selected \mathcal{D} and the remaining $\mathcal{U} \setminus \mathcal{D}$. A lower SRCC in \mathcal{D} indicates better failure identification performance. We find that, for all methods except random sampling, the selected images in \mathcal{D} are more difficult than the remaining ones. The proposed sampling-worthiness module delivers the best performance, identifying significantly more difficult samples. It is interesting to note that the failure identification performance of all methods, including the proposed failure predictor, can

TABLE VI
SRCC RESULTS OF THE PROPOSED SAMPLING-WORTHINESS MODULE AGAINST SIX COMPETING METHODS WITH AND WITHOUT THE DIVERSITY MEASURE. THE LARGE-SCALE UNLABELED SET \mathcal{U} IS SIMULATED WITH SPAQ [23]. A LOWER SRCC IN \mathcal{D} INDICATES A STRONGER CAPABILITY OF FAILURE IDENTIFICATION. RD: REPRESENTATIVENESS-DIVERSITY

Method	Without diversity		With diversity	
	\mathcal{D}	$\mathcal{U} \setminus \mathcal{D}$	\mathcal{D}	$\mathcal{U} \setminus \mathcal{D}$
Random sampling	0.8452	0.8382	0.8373	0.8383
Sampling by RD [36]	0.5932	0.8383	0.5575	0.8381
UNIQUE uncertainty [12]	0.5633	0.8397	0.5477	0.8400
Query by committee [52]	0.5487	0.8395	0.5352	0.8395
Core-set selection [34]	0.4968	0.8396	0.3796	0.8398
MC dropout [33]	0.4902	0.8376	0.3841	0.8379
Proposed	0.1894	0.8362	0.1413	0.8364

be enhanced by the incorporation of the diversity measure⁴.

c) Visual Results: Fig. 6 shows representative top- K images selected from SPAQ by the proposed sampling-worthiness module. Without the diversity constraint, the failure predictor alone is inclined to select difficult images of similar visual appearances, corresponding to the same underlying failure cause. When the diverse constraint is imposed, the selected images are more diverse in content and distortion.

D. Ablation Studies

To verify the flexibility and effectiveness of our sampling-worthiness module, we use it to spot diverse failures of six other BIQA models, including NIMA [10], KonCept512 [13], Fang2020 [23], HyperIQA [11], LinearityIQA [17], and MetaIQA+ [57]. The experimental setups and training protocols follow those described in Sec. IV-C.

Table VII shows the SRCC results of the proposed sampling-worthiness module in falsifying the six BIQA models on \mathcal{U} simulated with SPAQ. We find that the proposed module is able to spot difficult samples of the respective

⁴One subtlety is that each sampling strategy requires separate manual optimization of the trade-off parameter λ due to different scales between the two terms in Eq. (6).

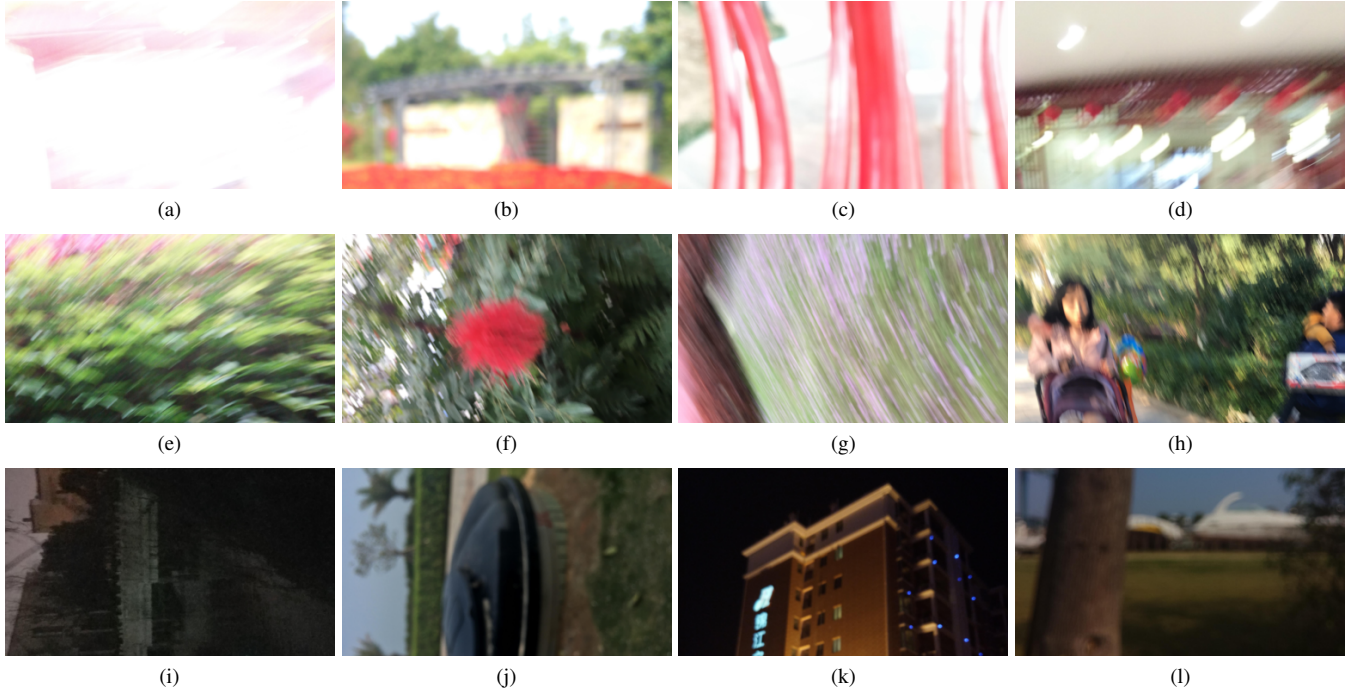


Fig. 7. Representative failure cases selected from SPAQ by the proposed sampling-worthiness module for (a)-(d) NIMA, (e)-(h) LinearityIQA, and (i)-(l) HyperIQA, respectively.

TABLE VII
SRCC RESULTS OF THE PROPOSED SAMPLING-WORTHINESS MODULE IN
FALSIFYING SIX BIQA MODELS ON THE UNLABELED DATASET \mathcal{U}
SIMULATED WITH SPAQ

Method	Without diversity		With diversity	
	\mathcal{D}	$\mathcal{U} \setminus \mathcal{D}$	\mathcal{D}	$\mathcal{U} \setminus \mathcal{D}$
NIMA [10]	0.0432	0.4019	0.0236	0.4010
KonCcept512 [13]	0.0358	0.8465	0.0054	0.8465
HyperIQA [11]	0.2675	0.8431	0.1216	0.8430
Fang2020 [23]	0.0690	0.7690	0.0336	0.7683
LinearityIQA [17]	0.1242	0.8737	0.1204	0.8737
MetaIQA+ [57]	0.1565	0.8470	0.0779	0.8473

BIQA model (even for Fang2020, which is originally trained on SPAQ). Fig. 7 shows representative failure cases of NIMA, LinearityIQA, and HyperIQA using the learned failure predictor alone. We observe that different BIQA models have their distinctive failure modes. For example, LinearityIQA fails to handle motion blur, while NIMA is weak at penalizing motion blur by camera shake.

We last investigate one interesting question: whether the failure predictor jointly trained with UNIQUE as the quality predictor is able to falsify the original UNIQUE (with and without the diversity measure). Specifically, joint training is performed by minimizing two fidelity losses⁵, one for quality assessment (in Eq. (3)) and the other for failure prediction (in Eq. (9)). The auxiliary task of failure prediction is down-weighted by a factor of 2 to emphasize the main task of quality assessment. The ResNet-34 backbone is initialized

⁵To simplify the implementation, we do not learn the uncertainty estimator $\sigma_w(\cdot)$, and instead set it to one.

TABLE VIII
SRCC RESULTS OF THE SAMPLING-WORTHINESS MODULE JOINTLY
TRAINED WITH UNIQUE, WHERE \mathcal{U} IS SIMULATED WITH SPAQ

Method	Without diversity		With diversity	
	\mathcal{D}	$\mathcal{U} \setminus \mathcal{D}$	\mathcal{D}	$\mathcal{U} \setminus \mathcal{D}$
Jointly trained UNIQUE	0.3518	0.8291	0.3046	0.8290
Original UNIQUE	0.3582	0.8386	0.3442	0.8387

with the weights pre-trained on ImageNet [71]. The last FC layer of UNIQUE and the failure predictor are initialized by He's method [69]. Other training protocols are the same as those described in Sec. IV-C, except that we perform a warm-up training in the first five epochs, where only randomly initialized layers are adjusted.

Table VIII shows the SRCC results of the sampling-worthiness module in falsifying the jointly trained UNIQUE and its original version. We find that the proposed module is able to expose different failures of the jointly trained UNIQUE, and such capability is transferable to falsify the original UNIQUE, although not as remarkable as the counterpart trained while fixing UNIQUE (see the last row of Table VI).

V. CONCLUSION AND FUTURE WORK

In this paper, we first conducted computational studies to reveal the overfitting problem and the easy dataset problem rooted in the current development of BIQA. We believe these arise because of the weak connections from model to data. Motivated by these, we have proposed a computational framework to integrate model-centric and data-centric IQA.

We also provided a specific instance by developing a sampling-worthiness module for difficulty and diversity quantification. Our module has been proved flexible and effective in spotting diverse failures of BIQA models.

In the future, we will improve the current sampling-worthiness module by developing better difficulty and diversity measures. We may also search for more efficient discrete optimization techniques to solve the subset selection problem in the context of IQA. Moreover, we will certainly leverage the sampling-worthiness module to construct a large-scale challenging IQA dataset, with the goal of facilitating the development of more generalizable IQA models. Last, we hope the proposed computational framework will inspire researchers in related fields to rethink the exciting future directions of IQA.

REFERENCES

- [1] Z. Wang and A. C. Bovik, *Modern Image Quality Assessment*. Morgan & Claypool Publishers, 2006. 1, 2
- [2] P. Ye, J. Kumar, L. Kang, and D. Doermann, “Unsupervised feature learning framework for no-reference image quality assessment,” in *IEEE Conference on Computer Vision and Pattern Recognition*, 2012, pp. 1098–1105. 1, 2
- [3] J. Xu, P. Ye, Q. Li, H. Du, Y. Liu, and D. Doermann, “Blind image quality assessment based on high order statistics aggregation,” *IEEE Transactions on Image Processing*, vol. 25, no. 9, pp. 4444–4457, 2016. 1
- [4] K. Ma, W. Liu, T. Liu, Z. Wang, and D. Tao, “dipIQ: Blind image quality assessment by learning-to-rank discriminable image pairs,” *IEEE Transactions on Image Processing*, vol. 26, no. 8, pp. 3951–3964, 2017. 1, 2
- [5] L. Kang, P. Ye, Y. Li, and D. Doermann, “Convolutional neural networks for no-reference image quality assessment,” in *IEEE Conference on Computer Vision and Pattern Recognition*, 2014, pp. 1733–1740. 1
- [6] K. Ma, W. Liu, K. Zhang, Z. Duanmu, Z. Wang, and W. Zuo, “End-to-end blind image quality assessment using deep neural networks,” *IEEE Transactions on Image Processing*, vol. 27, no. 3, pp. 1202–1213, 2017. 1
- [7] S. Bosse, D. Maniry, K.-R. Müller, T. Wiegand, and W. Samek, “Deep neural networks for no-reference and full-reference image quality assessment,” *IEEE Transactions on Image Processing*, vol. 27, no. 1, pp. 206–219, 2018. 1, 2, 3, 4
- [8] A. Mittal, A. K. Moorthy, and A. C. Bovik, “No-reference image quality assessment in the spatial domain,” *IEEE Transactions on Image Processing*, vol. 21, no. 12, pp. 4695–4708, 2012. 1, 2
- [9] X. Liu, J. van de Weijer, and A. D. Bagdanov, “RankIQA: Learning from rankings for no-reference image quality assessment,” in *IEEE International Conference on Computer Vision*, 2017, pp. 1040–1049. 1, 2, 3, 4
- [10] H. Talebi and P. Milanfar, “NIMA: Neural image assessment,” *IEEE Transactions on Image Processing*, vol. 27, no. 8, pp. 3998–4011, 2018. 1, 2, 3, 4, 9, 10
- [11] S. Su, Q. Yan, Y. Zhu, C. Zhang, X. Ge, J. Sun, and Y. Zhang, “Blindly assess image quality in the wild guided by a self-adaptive hyper network,” in *IEEE Conference on Computer Vision and Pattern Recognition*, 2020, pp. 3667–3676. 1, 2, 3, 4, 9, 10
- [12] W. Zhang, K. Ma, G. Zhai, and X. Yang, “Uncertainty-aware blind image quality assessment in the laboratory and wild,” *IEEE Transactions on Image Processing*, vol. 30, no. 258, pp. 3474–3486, 2021. 1, 2, 3, 4, 5, 6, 7, 8, 9
- [13] V. Hosu, H. Lin, T. Sziranyi, and D. Saupe, “KonIQ-10k: An ecologically valid database for deep learning of blind image quality assessment,” *IEEE Transactions on Image Processing*, vol. 29, no. 305, pp. 4041–4056, 2020. 1, 3, 4, 5, 6, 9, 10
- [14] W. Zhang, K. Ma, J. Yan, D. Deng, and Z. Wang, “Blind image quality assessment using a deep bilinear convolutional neural network,” *IEEE Transactions on Circuits and Systems for Video Technology*, vol. 30, no. 1, pp. 36–47, 2020. 1
- [15] F. Gao, D. Tao, X. Gao, and X. Li, “Learning to rank for blind image quality assessment,” *IEEE Transactions on Neural Networks and Learning Systems*, vol. 26, no. 10, pp. 2275–2290, 2015. 1
- [16] T.-Y. Liu, *Learning to Rank for Information Retrieval*. Springer Science & Business Media, 2011. 1, 2
- [17] D. Li, T. Jiang, and M. Jiang, “Norm-in-norm loss with faster convergence and better performance for image quality assessment,” in *ACM International Conference on Multimedia*, 2020, pp. 789–797. 1, 2, 3, 4, 9, 10
- [18] Z. Wang, D. Li, and K. Ma, “Semi-supervised deep ensembles for blind image quality assessment,” in *International Joint Conference on Artificial Intelligence Workshop on Weakly Supervised Representation Learning*, 2021, pp. 1–6. 1
- [19] M. Li, “Scaling distributed machine learning with system and algorithm co-design,” Ph.D. dissertation, Carnegie Mellon University, 2017. 1
- [20] H. R. Sheikh, M. F. Sabir, and A. C. Bovik, “A statistical evaluation of recent full reference image quality assessment algorithms,” *IEEE Transactions on Image Processing*, vol. 15, no. 11, pp. 3440–3451, 2006. 1, 2, 3
- [21] A. Ciancio, A. L. N. T. da Costa, E. A. B. da Silva, A. Said, R. Samadani, and P. Obrador, “No-reference blur assessment of digital pictures based on multifeature classifiers,” *IEEE Transactions on Image Processing*, vol. 20, no. 1, pp. 64–75, 2011. 1, 3, 4, 5, 6
- [22] D. Ghadiyaram and A. C. Bovik, “Massive online crowdsourced study of subjective and objective picture quality,” *IEEE Transactions on Image Processing*, vol. 25, no. 1, pp. 372–387, 2016. 1, 2, 3, 4, 5, 6
- [23] Y. Fang, H. Zhu, Y. Zeng, K. Ma, and Z. Wang, “Perceptual quality assessment of smartphone photography,” in *IEEE Conference on Computer Vision and Pattern Recognition*, 2020, pp. 3677–3686. 1, 2, 3, 4, 5, 6, 9, 10
- [24] R. K. Mantiuk, A. Tomaszewska, and R. Mantiuk, “Comparison of four subjective methods for image quality assessment,” *Computer Graphics Forum*, vol. 31, no. 8, pp. 2478–2491, 2012. 1
- [25] Q. Xu, Q. Huang, T. Jiang, B. Yan, W. Lin, and Y. Yao, “HodgeRank on random graphs for subjective video quality assessment,” *IEEE Transactions on Multimedia*, vol. 14, no. 3, pp. 844–857, 2012. 1, 2
- [26] P. Ye and D. Doermann, “Active sampling for subjective image quality assessment,” in *IEEE Conference on Computer Vision and Pattern Recognition*, 2014, pp. 4249–4256. 1, 2
- [27] V. Vonikakis, R. Subramanian, J. Arnfred, and S. Winkler, “A probabilistic approach to people-centric photo selection and sequencing,” *IEEE Transactions on Multimedia*, vol. 19, no. 11, pp. 2609–2624, 2017. 2, 3
- [28] P. Cao, Z. Wang, and K. Ma, “Debiased subjective assessment of real-world image enhancement,” in *IEEE Conference on Computer Vision and Pattern Recognition*, 2021, pp. 711–721. 2, 3
- [29] Z. Wang and E. P. Simoncelli, “Maximum differentiation (MAD) competition: A methodology for comparing computational models of perceptual quantities,” *Journal of Vision*, vol. 8, no. 12, pp. 1–13, 2008. 2, 3
- [30] H. Wang, T. Chen, Z. Wang, and K. Ma, “I am going MAD: Maximum discrepancy competition for comparing classifiers adaptively,” in *International Conference on Learning Representations*, 2020, pp. 1–13. 2
- [31] K. Ding, K. Ma, S. Wang, and E. P. Simoncelli, “Comparison of full-reference image quality models for optimization of image processing systems,” *International Journal of Computer Vision*, vol. 129, no. 4, pp. 1258–1281, 2021. 2
- [32] K. Simonyan and A. Zisserman, “Very deep convolutional networks for large-scale image recognition,” in *International Conference on Learning Representations*, 2015, pp. 1–14. 2, 8
- [33] R. Pop and P. Fulop, “Deep ensemble Bayesian active learning: Addressing the mode collapse issue in Monte Carlo dropout via ensembles,” *arXiv preprint arXiv:1811.03897*, 2018. 2, 8, 9
- [34] O. Sener and S. Savarese, “Active learning for convolutional neural networks: A core-set approach,” in *International Conference on Learning Representations*, 2018, pp. 1–13. 2, 8, 9
- [35] R. Burbidge, J. J. Rowland, and R. D. King, “Active learning for regression based on query by committee,” in *International Conference on Intelligent Data Engineering and Automated Learning*, 2007, pp. 209–218. 2
- [36] D. Wu, “Pool-based sequential active learning for regression,” *IEEE Transactions on Neural Networks and Learning Systems*, vol. 30, no. 5, pp. 1348–1359, 2019. 2, 8, 9
- [37] A. K. Moorthy and A. C. Bovik, “Blind image quality assessment: From natural scene statistics to perceptual quality,” *IEEE Transactions on Image Processing*, vol. 20, no. 12, pp. 3350–3364, 2011. 2
- [38] M. A. Saad, A. C. Bovik, and C. Charrier, “Blind image quality assessment: A natural scene statistics approach in the DCT domain,”

IEEE Transactions on Image Processing, vol. 21, no. 8, pp. 3339–3352, 2012. 2

[39] M.-F. Tsai, T.-Y. Liu, T. Qin, H.-H. Chen, and W.-Y. Ma, “FRank: A ranking method with fidelity loss,” in *International ACM SIGIR Conference on Research and Development in Information Retrieval*, 2007, pp. 383–390. 2, 3

[40] E. C. Larson and D. M. Chandler, “Most apparent distortion: Full-reference image quality assessment and the role of strategy,” *Journal of Electronic Imaging*, vol. 19, no. 1, pp. 1–21, 2010. 2, 3

[41] N. Ponomarenko, L. Jin, O. Ieremeiev, V. Lukin, K. Egiazarian, J. Astola, B. Vozel, K. Chehdi, M. Carli, F. Battisti, and C.-C. J. Kuo, “Image database TID2013: Peculiarities, results and perspectives,” *Signal Processing: Image Communication*, vol. 30, no. 3, pp. 57–77, 2015. 2

[42] ITU-R Recommendation, “BT.500-14: Methodologies for the subjective assessment of the quality of television images,” 2019. [Online]. Available: https://www.itu.int/dms_pubrec/itu-r/rec/bt/R-REC-BT.500-14-201910-I!!PDF-E.pdf 2, 5

[43] H. Men, H. Lin, M. Jenadeleh, and D. Saupe, “Subjective image quality assessment with boosted triplet comparisons,” *IEEE Access*, vol. 9, pp. 138 939–138 975, 2021. 2

[44] K.-T. Chen, C.-C. Wu, Y.-C. Chang, and C.-L. Lei, “A crowdsourcing QoE evaluation framework for multimedia content,” in *ACM International Conference on Multimedia*, 2009, pp. 491–500. 2

[45] N. Ponomarenko, V. Lukin, A. Zelensky, K. Egiazarian, M. Carli, and F. Battisti, “TID2008 - A database for evaluation of full-reference visual quality assessment metrics,” *Advances of Modern Radioelectronics*, vol. 10, no. 4, pp. 30–45, 2009. 3

[46] Z. Ying, H. Niu, P. Gupta, D. Mahajan, D. Ghadiyaram, and A. C. Bovik, “From patches to pictures (PaQ-2-PiQ): Mapping the perceptual space of picture quality,” in *IEEE Conference on Computer Vision and Pattern Recognition*, 2020, pp. 3575–3585. 3

[47] B. Settles, “Active learning literature survey,” University of Wisconsin–Madison, Tech. Rep., 2010. 3

[48] P. Ren, Y. Xiao, X. Chang, P.-Y. Huang, Z. Li, B. B. Gupta, X. Chen, and X. Wang, “A survey of deep active learning,” *ACM Computing Surveys*, vol. 54, no. 9, pp. 1–40, 2021. 3

[49] Z. Wang and K. Ma, “Active fine-tuning from gMAD examples improves blind image quality assessment,” *IEEE Transactions on Pattern Analysis and Machine Intelligence*, 2021, To Appear. 3

[50] Z. Wang, H. Wang, T. Chen, Z. Wang, and K. Ma, “Troubleshooting blind image quality models in the wild,” in *IEEE Conference on Computer Vision and Pattern Recognition*, 2021, pp. 16 256–16 265. 3

[51] D. A. Cohn, Z. Ghahramani, and M. I. Jordan, “Active learning with statistical models,” *Journal of Artificial Intelligence Research*, vol. 4, no. 1, pp. 129–145, 1996. 3

[52] H. S. H. S. Seung, M. Opper, “Query by committee,” in *Annual Workshop on Computational Learning Theory*, 1992, pp. 287–297. 3, 8, 9

[53] W. Cai, Y. Zhang, and J. Zhou, “Maximizing expected model change for active learning in regression,” in *IEEE International Conference on Data Mining*, 2013, pp. 51–60. 3

[54] W. Scheirer and T. Boult, “A fusion-based approach to enhancing multi-modal biometric recognition system failure prediction and overall performance,” in *IEEE International Conference on Biometrics: Theory, Applications and Systems*, 2008, pp. 1–7. 3

[55] P. Zhang, J. Wang, A. Farhadi, M. Hebert, and D. Parikh, “Predicting failures of vision systems,” in *IEEE Conference on Computer Vision and Pattern Recognition*, 2014, pp. 3566–3573. 3

[56] K. He, X. Zhang, S. Ren, and J. Sun, “Deep residual learning for image recognition,” in *IEEE Conference on Computer Vision and Pattern Recognition*, 2016, pp. 770–778. 3, 8

[57] H. Zhu, L. Li, J. Wu, W. Dong, and G. Shi, “Generalizable no-reference image quality assessment via deep meta-learning,” *IEEE Transactions on Circuits and Systems for Video Technology*, vol. 32, no. 3, pp. 1048–1060, 2022. 3, 4, 5, 9, 10

[58] I. Goodfellow, Y. Bengio, and A. Courville, *Deep Learning*. MIT Press, 2016. 3

[59] K. Ma, Z. Duanmu, Z. Wang, Q. Wu, W. Liu, H. Yong, H. Li, and L. Zhang, “Group maximum differentiation competition: Model comparison with few samples,” *IEEE Transactions on Pattern Analysis and Machine Intelligence*, vol. 42, no. 4, pp. 851–864, 2020. 3, 4

[60] C. D. Manning, P. Raghavan, and H. Schütze, *Introduction to Information Retrieval*. Cambridge University Press, 2008. 5

[61] T. L. Saaty and L. G. Vargas, “Inconsistency and rank preservation,” *Journal of Mathematical Psychology*, vol. 28, no. 2, pp. 205–214, 1984. 5

[62] G. Davis, S. Mallat, and M. Avellaneda, “Adaptive greedy approximations,” *Constructive Approximation*, vol. 13, no. 1, pp. 57–98, 1997. 7

[63] B. K. Natarajan, “Sparse approximate solutions to linear systems,” *SIAM Journal on Computing*, vol. 24, no. 2, pp. 227–234, 1995. 7

[64] M. Welling, “Herding dynamical weights to learn,” in *International Conference on Machine Learning*, 2009, pp. 1121–1128. 7

[65] E. Elhamifar and R. Vidal, “Sparse subspace clustering: Algorithm, theory, and applications,” *IEEE Transactions on Pattern Analysis and Machine Intelligence*, vol. 35, no. 11, pp. 2765–2781, 2013. 7

[66] I. Misra, A. Shrivastava, and M. Hebert, “Data-driven exemplar model selection,” in *IEEE Winter Conference on Applications of Computer Vision*, 2014, pp. 339–346. 7

[67] D. Yoo and I. S. Kweon, “Learning loss for active learning,” in *IEEE Conference on Computer Vision and Pattern Recognition*, 2019, pp. 93–102. 7, 8

[68] C.-C. Kuo, F. Glover, and K. S. Dhir, “Analyzing and modeling the maximum diversity problem by zero-one programming,” *Decision Sciences*, vol. 24, no. 6, pp. 1171–1185, 1993. 8

[69] K. He, X. Zhang, S. Ren, and J. Sun, “Delving deep into rectifiers: Surpassing human-level performance on ImageNet classification,” in *IEEE International Conference on Computer Vision*, 2015, pp. 1026–1034. 8, 10

[70] D. P. Kingma and J. Ba, “Adam: A method for stochastic optimization,” in *International Conference on Learning Representations*, 2015, pp. 1–15. 8

[71] J. Deng, W. Dong, R. Socher, L.-J. Li, K. Li, and L. Fei-Fei, “ImageNet: A large-scale hierarchical image database,” in *IEEE Conference on Computer Vision and Pattern Recognition*, 2009, pp. 248–255. 10